

# Electrostatic Protein Immobilization Using Charged Polyacrylamide Gels and Cationic Detergent Microfluidic Western Blotting

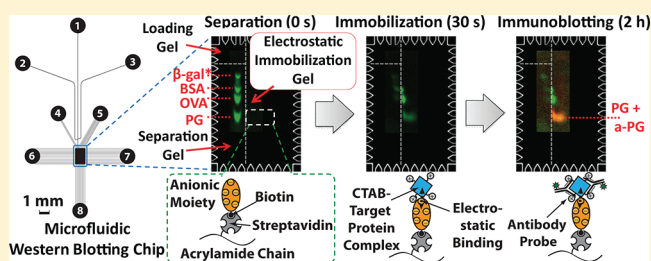
Dohyun Kim,<sup>†</sup> Kelly Karns,<sup>‡</sup> Samuel Q. Tia,<sup>‡</sup> Mei He,<sup>†</sup> and Amy E. Herr<sup>\*,†,‡</sup>

<sup>†</sup>Department of Bioengineering, University of California, Berkeley, 342 Stanley Hall, Berkeley, California 94720, United States

<sup>‡</sup>The UC Berkeley – UCSF Graduate Program in Bioengineering, Berkeley, California 94720, United States

## Supporting Information

**ABSTRACT:** We report a novel protein immobilization matrix for fully integrated microfluidic Western blotting (WB). The electrostatic immobilization gel (EIG) enables immobilization of all proteins sized using cetyl trimethylammonium bromide polyacrylamide gel electrophoresis (CTAB-PAGE), for subsequent electrophoretic probing with detection affinity reagents (e.g., labeled antibodies). The “pan-analyte” capture strategy introduced here uses polyacrylamide gel grafted with concentrated point charges (zwitterionic macromolecules), in contrast to existing microfluidic WB strategies that rely on a sandwich immunoassay format for analyte immobilization and detection. Sandwich approaches limit analyte immobilization to capture of only a priori known targets. A charge interaction mechanism study supports the hypothesis that electrostatic interaction plays a major role in analyte immobilization on the EIG. We note that protein capture efficiency depends on both the concentration of copolymerized charges and ionic strength of the gel buffer. We demonstrate pan-analyte immobilization of sized CTAB-laden model proteins (protein G, ovalbumin, bovine serum albumin,  $\beta$ -galactosidase, lactoferrin) on the EIG with initial capture efficiencies ranging from 21 to 100%. Target proteins fixed on the EIG (protein G, lactoferrin) are detected using antibody probes with signal-to-noise ratios of 34 to 275. The approach advances protein immunoblotting performance through 200 $\times$  reduction on sample consumption, 12 $\times$  reduction in assay duration, and automated assay operation, compared to slab-gel WB. Using the microfluidic WB assay, assessment of lactoferrin in human tear fluid is demonstrated with a goal of advancing toward nonbiopsy-based diagnosis of Sjögren’s Syndrome, an autoimmune disease.



In biomedicine alone, proteins are utilized for a wide variety of applications, including roles as therapeutic targets and diagnostic disease biomarkers.<sup>1</sup> To tease apart protein characteristics important to each role (e.g., expression level variation, co/post-translational modifications, and complex formation), Western blotting (WB) and protein microarrays have emerged as indispensable analytical tools. WB relies on high resolution electrophoretic protein separations to reduce sample complexity, as a first stage.<sup>2</sup> In a second stage, antibody-based probing of the sized proteins transferred to a membrane<sup>3</sup> allows correlation between a known antibody signal and molecular mass ( $M_r$ ), thus conferring nearly unmatched analytical specificity.<sup>4</sup> While protein microarrays do not yield the specificity of WB, microarray platforms quantify numerous proteins in one assay from limited sample material.<sup>5</sup> In both analytical platforms, effective immobilization of proteins on suitable solid phase materials is critical as immobilization efficiency is directly correlated to assay performance (e.g., analytical sensitivity, background levels, reproducibility).<sup>1</sup>

Polyvinylidene fluoride (PVDF), polystyrene (PS), and nitrocellulose (NC) membranes, used in microarray development, are limited to a low density of printed proteins (PVDF, PS) and high autofluorescence (NC).<sup>6</sup> Consequently, activated glass slides have gained popularity as protein immobilization

substrates for microarrays.<sup>5</sup> Recently, polyacrylamide (PA) gel has drawn much attention as a protein immobilization matrix for microarrays<sup>7,8</sup> as well for in-gel protein detection of WB.<sup>9,10</sup> PA gels afford an attractive set of properties: large immobilization capacity (3-D polymer networks);<sup>11</sup> excellent optical properties for imaging (transparency and weak autofluorescence);<sup>1,11</sup> a hydrophilic environment retaining protein/antibody activities;<sup>8</sup> low nonspecific protein adsorption;<sup>1</sup> widely available chemical modifications for effective immobilization (e.g., aldehyde for covalent linkage);<sup>1</sup> facile incorporation of functional biomolecules (e.g., DNA, protein, glycan);<sup>8</sup> easy modification of physical properties (e.g., porosity);<sup>8</sup> and lastly, straightforward microscale photopatterning using photoinitiators.<sup>12–15</sup> Strategies for protein immobilization to a matrix include covalent bonding (e.g., NHS-ester to amino group), bioaffinity interaction (e.g., biotin to avidin), and physical adsorption (e.g., electrostatic).<sup>1</sup> Physical adsorption offers unique advantages over the other methods: simplicity (no multiple-step chemistries);<sup>1</sup> reversibility (matrix reusable after elution of immobilized proteins);<sup>16</sup> and a wide

Received: January 1, 2012

Accepted: January 26, 2012

Published: January 26, 2012

range of buffer compatibilities, unlike covalent bonding where widely used amine-containing buffers (e.g., Tris-glycine) interfere with immobilization chemistries. If the benefits of PA gels and electrostatic adsorption are combined, solid supports for effective protein immobilization can be yielded.

Although slab-gel WB is one of the most widely used methods in life science and biotechnology,<sup>17</sup> the WB has been changed little since its introduction in 1979:<sup>3</sup> the vast majority of research utilizes the benchtop wet format that consumes copious samples (1–40  $\mu\text{g}$ ), runs slowly (1–2 days), and requires labor-intensive manual operation of multiple disconnected steps. Recently, notable improvements have been made to the slab-gel WB. Microwestern arrays offer a combination of WB and microarray technology for excellent multiplexing capability.<sup>4</sup> However, this approach takes longer than the slab-gel WB and requires manual handling of separate instruments including an expensive microarrayer. In a “ $\mu\text{WB}$ ” method,<sup>18</sup> a PDMS microfluidic network is manually overlaid over protein blots on a membrane to perform multiplexed immunoblotting. Prior to the immunoblotting, conventional sodium dodecyl sulfate (SDS)-polyacrylamide gel electrophoresis (PAGE) and electrotransfer steps are completed manually. Recent work in capillary-based systems includes concatenation of capillary gel electrophoresis with blotting of effluent analyte peaks on a moving blotting membrane.<sup>17</sup> To minimize manual handling and integrate multiple assay steps in one instrument, our lab has recently introduced a completely microfluidic design strategy for WB.<sup>12–15</sup> After on-chip native PAGE, protein peaks are transferred through antibodies immobilized in a polyacrylamide gel.<sup>13–15</sup> All functional gel elements are housed in a microchamber ( $\sim 1 \times \sim 1 \text{ mm}^2$ ) of a glass chip. Owing to automated electrophoretic protein manipulation, the entire WB procedure is completed in  $\sim 5$  min with minimal manual intervention. Sample consumption is also miniscule (0.01 to 0.5  $\mu\text{g}$ ). Although performance gains are made, the microfluidic WB approaches to date have critical limitations.<sup>12–15</sup> Chiefly, by relying on a priori immobilized antibodies, only explicitly targeted proteins, not all sized species, are captured and detected. Moreover, detergent-based separations such as SDS-PAGE are difficult to integrate with subsequent antibody-based protein peak capture, owing to reduced affinity between surfactant-coated proteins and the immobilized antibodies.

To surmount protein immobilization shortcomings that have limited advances in completely integrated microfluidic WB, we introduce and characterize a novel protein immobilization based on electrostatic interaction with charge-functionalized PA gels. We elucidate the nature of strong protein immobilization in the presence of surfactant, through study of the immobilization mechanism. The unique features of the electrostatic immobilization gel (EIG) introduced here include adjustable protein immobilization strength and effective protein capture achieved by copolymerization of charged zwitterionic macromolecules. In a second contribution, we integrate the EIG with surfactant-based protein sizing to broaden the relevance and advance the capabilities of microfluidic WB. The EIG is used as a protein immobilization matrix after cationic detergent CTAB (cetyl trimethylammonium bromide)-based protein sizing.<sup>19–24</sup> Importantly, the EIG enables pan-analyte (nonspecific) capture of detergent-treated proteins via electrostatic interaction while conserving  $M_r$  information and allowing subsequent target probing by electrophoretically introduced antibodies. The EIG is integrated with a loading

gel and separation gel in a 2-D microchamber architecture<sup>12–15</sup> through photopatterning. Thus, no discernible material or information losses arise at the interface of neighboring gel regions unlike macroscale WB. CTAB-PAGE offers log–linear  $M_r$  vs mobility information at sizing completion while retaining some degree of antibody affinity to CTAB-coated proteins,<sup>22–24</sup> thus obviating explicit protein renaturation steps. Further, CTAB-PAGE offers a log–linear  $M_r$  vs mobility range wider than SDS-PAGE<sup>22</sup> and can accurately size proteins migrating anomalously in SDS-PAGE.<sup>19,21,23,24</sup> Using the new platform technology, we successfully assay lactoferrin (LF), a putative biomarker of autoimmune dysfunction, in a complex biological matrix (i.e., human tear fluid). Our new microfluidic approach is a promising WB technology for protein research in an automated, low-sample consuming and high-throughput format while maintaining the hallmark high specificity and assay versatility (e.g., various postsizing protein staining methods) of conventional WB.

## ■ EXPERIMENTAL SECTION

**Reagents and Samples.** Protein G (PG, 20 kDa), ovalbumin (OVA, 45 kDa), and bovine serum albumin (BSA, 68 kDa) were from Invitrogen (Carlsbad, CA). Phosphorylase b (97.2 kDa),  $\alpha$ -actinin ( $\alpha\text{A}$ , 95 kDa), and  $\beta$ -gal\* (indicates  $\beta$ -galactosidase monomer, 116 kDa, not to be confused with tetramer “ $\beta$ -gal”) were from Sigma (St. Louis, MO). S100B (10.5 kDa) and lactoferrin (LF, 78 kDa) were from Abcam (Cambridge, MA). All the proteins were purchased with fluorophore conjugation or conjugated in-house with Alexa Fluor 488 (Invitrogen) following manufacturer’s instruction. Rabbit polyclonal anti-PG (Abcam) and goat polyclonal anti-LF (Bethyl Laboratories, Montgomery, TX) were conjugated in-house with Alexa Fluor 568 (Invitrogen). The proteins and antibodies were all solubilized in Tricine-arginine (TA) buffer (0.13 $\times$ , 1 $\times$ , 7.57 $\times$  concentrations depending on assay). For 1 $\times$  TA buffer, 125 mM Tricine is brought to pH 8.2 using 1 M arginine stock solution (all from Sigma). For LF analysis, LF in healthy patient tears was depleted using immunoprecipitation (see Karns and Herr<sup>25</sup> and Supporting Information therein for detail) and LF of known concentration was spiked into the processed tears. CTAB (Sigma, 0.1–0.2% for purified samples and 0.7% for tear fluid) was added to the protein samples 15 min before loading.

### Fabrication of the EIG in a Glass Microfluidic Device.

The fabrication processes for wet etched glass microfluidic chips (Figure S-1a, Supporting Information) and photopatterning of PA gel regions in a glass microdevice (Figure S-1b, Supporting Information) are described in the Supporting Information and previous studies.<sup>12–15</sup> All PA gels used in this study were photopolymerized using acrylamide/bisacrylamide (Sigma, 3.3% w/w cross-linker) with 0.2% w/v photoinitiator (VA-086, Wako Chemical, Richmond, VA). To fabricate EIGs (Figure 1a) for electrostatic protein immobilization, charged moieties were included in the polymer precursor solution. For the charge density study, the EIG was copolymerized with zwitterionic macromolecules:  $\beta$ -gal ( $\beta$ -galactosidase tetramer, 465 kDa, Sigma) or IgG (Abcam, mouse monoclonal anti-CRP). For comparison, acrylamido buffer (Immobiline, pK = 3.6, GE Healthcare, Pittsburgh, PA) was also copolymerized. Biotinylated  $\beta$ -gal and IgG were copolymerized in PA gel using a 3.8  $\mu\text{M}$  streptavidin acrylamide linker (Invitrogen) in 1 $\times$  TA buffer. While  $\beta$ -gal was purchased biotinylated, IgG was biotinylated using a commercial biotinylation kit (Pierce

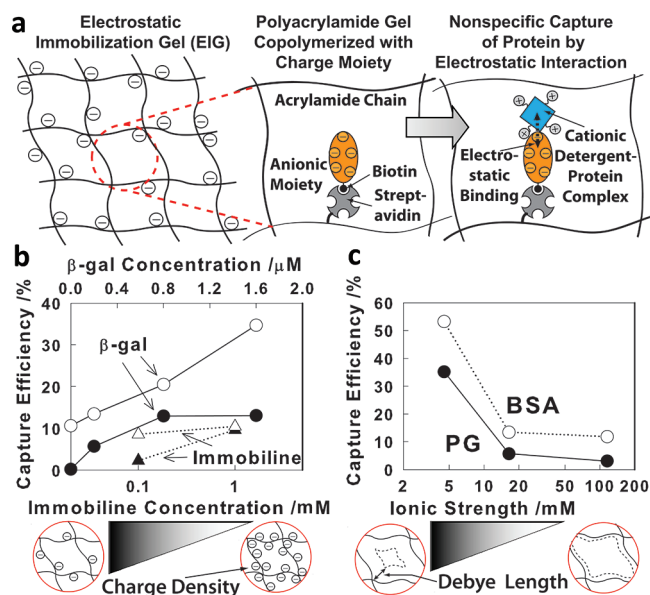


**Figure 1.** Charged PA gel allows electrostatic immobilization of surfactant-coated proteins. (a) The EIG is composed of an anionic capture moiety copolymerized using streptavidin–biotin linker (not to scale). Positively charged CTAB–protein complexes are electrophoresed to the EIG and immobilized. Varying (b) charge and (c) buffer properties allows investigation of protein immobilization on the EIG. Protein retention is assessed before and after protein immobilization under varying EIG conditions. (b) Charge density of the EIG was varied by modifying copolymerized  $\beta$ -gal concentration (circle) or Immobiline concentration (triangle). Open symbols denote BSA and solid symbols denote PG. (c) Debye length of the EIG pores was varied by modifying ionic strength of gel buffer.

Protein Research, Rockford, IL). For the EIG characterization study, monomer content (T) was 3%T, 6%T, and 9%T for the loading gel, separation gel, and EIG, respectively (Figure S-2a, Supporting Information). All PA gels were polymerized under UV exposure (power = 13 mW·cm<sup>-2</sup>, exposure time = 8 min).

For microfluidic WB assays (Figure 2), the same gel composition and exposure conditions were used for the loading and separation gels. All gel precursors were prepared in 1× TA buffer. For the WB assay of PG, the EIG was 9%T PA gel copolymerized with 1.6  $\mu$ M  $\beta$ -gal under the same exposure condition. For the WB assay of LF, the EIG was 6%T PA gel (1.6  $\mu$ M  $\beta$ -gal) polymerized under a lower exposure power (5 mW·cm<sup>-2</sup>) and for a slightly longer exposure time (10.5 min). The exposure power was lowered to mitigate sudden pore size reduction at the interface between EIG and separation gel.<sup>26</sup> At a high exposure power (13 mW·cm<sup>-2</sup>), nonspecific pseudoimmobilization of abundant tear proteins<sup>27</sup> at the interface resulted in a strong background signal in LF immunoblotting.

**Automated Microfluidic Assay Control.** Electrophoretic protein migration is controlled by applying a sequence of voltages and currents via 8 access holes (Figure 2a) using a custom built, 8 channel high-voltage sequencer. A typical voltage/current program for the EIG characterization (protein loading, separation, transfer) and WB assay (protein loading, separation, transfer, blocking, immunoblotting) is shown in Table S-1, Supporting Information. A major difference in the assay procedure from previous work<sup>12–15</sup> is “priming” of the separation axis (Figure 2b) with CTAB.<sup>21</sup> CTAB is not added to the gel precursor solution prior to photopolymerization

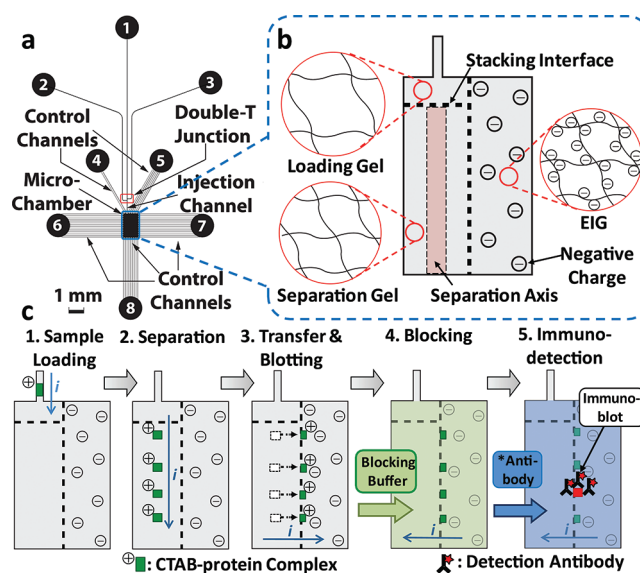


**Figure 2.** Charged PA gel for postsizing pan-analyte capture in a microfluidic WB. (a) A central microchamber is surrounded by microchannels for sample/reagent introduction and transport with minimal dispersion using electric field control<sup>31</sup> (access holes #1 to #8). (b) To integrate sizing with nonspecific protein capture, photopatterning is used to fabricate spatially distinct functional PA gel regions: loading gel for protein loading, separation gel for CTAB-PAGE, and EIG for protein transfer and immobilization followed by antibody probing. (c) Multiple WB assay steps are integrated in the microchamber: Step 1, protein sample plug injection; Step 2, CTAB-PAGE protein separation and sizing; Step 3, electrotransfer and nonspecific blotting of separated proteins in the EIG; Step 4, blocking of nonspecific antibody binding sites on EIG; Step 5, injection of antibody probe and readout of immunoblot.

because CTAB interferes with polymerization.<sup>20–22</sup> CTAB (0.1–0.5%, depending on assay) is loaded to access holes #1, #2, and #3 and electrophoretically introduced into sample loading channels (from access hole #2 and #3) for 10 min. Then, CTAB is injected as a narrow band to define the separation axis for 10 min before protein sample loading. Addition of detergent in the sample loading channels and along the separation axis prevents unwanted interaction between positively charged CTAB–protein complexes and hydrolyzed PA gel matrix,<sup>28–30</sup> which would result in band dispersion.

**Fluorescence Imaging and Image Analysis.** An epifluorescence microscope (IX-70, Olympus, Center Valley, PA) was used for data collection via a Peltier-cooled CCD camera (CoolSNAP HQ<sup>2</sup>, 1392 × 1030 resolution, Photometrics, Tucson, AZ). Imaging was conducted using a 100 W mercury lamp (Olympus), 10× objective (UPlanFL, NA = 0.3, Olympus), 0.63× demagnifier (Diagnostic Instruments Inc., Sterling Heights, MI), and XF100-3 and XF111-2 filter sets (Omega Optical, Brattleboro, VT). Images were captured under 200 ms exposure time and 4 × 4 pixel binning. Image analysis used ImageJ software (NIH, Bethesda, Maryland) with background subtraction (50 pixel rolling-ball radius). Protein material was quantified using the area under the curve (AUC) from fluorescence micrographs. The curve, a function of  $x$ , is generated from a  $y$ -axis intensity average of the two-dimensional fluorescence image. Protein capture efficiency was calculated from material retention on the EIG. Material retention was defined as the ratio (%) of the fluorescence signal from protein zones before (in the separation gel) and after

immobilization (in the EIG) as seen in Figure S-2c, Supporting Information.

## RESULTS AND DISCUSSION

**Characterization of EIG for Protein Immobilization and Binding Mechanism Study.** To yield a versatile photopatternable material for strong analyte immobilization,  $\beta$ -gal was incorporated into a photopatterned PA gel (Figure 1a). The total number of negative surface charges on  $\beta$ -gal is significant ( $-160e$ ) in TA buffer (pH = 8.2)<sup>32</sup> owing to the low pI point (4.61) and large  $M_r$  (465 kDa) of the  $\beta$ -gal macromolecule. To fully characterize protein immobilization on the EIG, two physicochemical properties, charge density and buffer ionic strength, were varied and protein capture efficiency was quantified using model proteins PG (600 nM) and BSA (180 nM). We first assessed protein capture efficiency for an EIG created by charge grafting of  $\beta$ -gal at increasing concentrations. Four WB chips with EIG copolymerized  $\beta$ -gal concentration of 0, 0.2, 0.8, and 1.6  $\mu$ M were fabricated. PG and BSA were solubilized in 0.1% CTAB and loaded through the loading gel, separated into two bands in the separation gel, and transferred and immobilized on the EIG (Figure S-2b, Supporting Information). After immobilization, a horizontal electric field was applied for 30 min to remove residual and free CTAB from the EIG. Material retention for both PG (solid circle) and BSA (open circle) increased with increasing charge density up to 1.6  $\mu$ M  $\beta$ -gal with PG capture efficiencies plateauing at this concentration (Figure 1b). The result agreed with previous studies, where protein capture improved with increasing charge density on the interacting surface of opposite polarity.<sup>33</sup> We also noted immobilization of BSA even with 0  $\mu$ M  $\beta$ -gal in the EIG, attributed to negative charges resulting from PA hydrolysis in the alkaline buffer conditions.<sup>28–30</sup>

After observing effective protein capture in PA gels copolymerized with  $\beta$ -gal, we next compared capture efficiencies with an alternate approach to charge grafting. Immobilines are often used to create stationary charge gradient in PA gels.<sup>34</sup> We employed acidic Immobilines (pK = 3.6) to impart negative charges to the EIG at pH 8.2. As shown in Figure 1b, for 0.1 mM Immobiline, the capture efficiencies for both PG (2.2%, closed triangle) and BSA (8.5%, open triangle) were close to that of the negative control for the  $\beta$ -gal EIG (0  $\mu$ M  $\beta$ -gal, circles). At an increased Immobiline concentration of 1 mM, high stationary charges resulted in concentration polarization (i.e., electrical current at access hole #5 dropped to 45% of the initial value immediately), making electrophoretic protein immobilization assay challenging. At 1 mM Immobiline, the capture efficiency for PG was similar to 0.5  $\mu$ M  $\beta$ -gal (9.6%), while that for BSA remained similar to the 0  $\mu$ M  $\beta$ -gal case (10.4%). At higher charge densities (e.g., 10 mM Immobiline), protein immobilization could not be performed, owing to strong concentration polarization (i.e., the current at access hole #5 dropped to <10% of the initial value immediately). Noting that the net charge density on the 0.5  $\mu$ M  $\beta$ -gal EIG was estimated to be 0.08 mM, the  $\beta$ -gal EIG provided much stronger protein capture than the Immobiline EIG for a given charge density. We attribute the stronger capture to the charge distribution in the gel pores. Dimensional analysis indicates that  $\sim 1$  molecule of  $\beta$ -gal is immobilized in each pore for a 0.5  $\mu$ M  $\beta$ -gal EIG (6%T);<sup>35</sup>  $\beta$ -gal acts as a concentrated point charge ( $-160e$  per molecule).<sup>32</sup> In contrast,  $\sim 140$  singly charged Immobiline molecules (for 1 mM concentration) are likely distributed throughout the pores.

The electrostatic interaction with a CTAB–protein complex thus may be more diffuse in origin, and the resultant force may be smaller than the  $\beta$ -gal case (Figure S-3, Supporting Information). To further investigate this hypothesis, EIG copolymerized with 1.6  $\mu$ M of IgG (150 kDa, pI point can be as low as 5.5)<sup>36</sup> was used to immobilize BSA. The capture efficiency for BSA was 76.7%, 29 s after immobilization. At the same elapsed time, the capture efficiency for BSA was 55.0% on 1.6  $\mu$ M  $\beta$ -gal EIG. Although the IgG EIG yielded more efficient capture of BSA, the  $\beta$ -gal EIG was chosen for the charged moiety, owing to cross-reactivity of IgG with specific targets. In summary, copolymerization of  $\beta$ -gal with the PA gel yielded a strong, stationary charge bearing region.

We next varied the buffer ionic strength in the EIG to assess the impact of the electric double layer (EDL) in the EIG pores on protein capture. Variation of ionic strength decouples electrostatic contributions from other binding mechanisms (e.g., hydrophobic interactions<sup>37</sup>), thus allowing assessment of electrostatic interaction as the dominant binding mechanism.<sup>38,39</sup> As Debye length (EDL thickness) decreases with increasing buffer ionic strength, protein capture efficiencies are hypothesized to diminish, owing to enhanced charge shielding.<sup>33,40</sup> Three EIGs with a fixed  $\beta$ -gal concentration (0.2  $\mu$ M) but increasing ionic strength TA buffer (0.13 $\times$ , 1 $\times$ , and 7.57 $\times$ ) were fabricated, and protein capture was characterized. The ionic strengths for the three buffer conditions were 115.4, 16.4, and 4.5 mM for 7.57 $\times$ , 1.0 $\times$ , and 0.13 $\times$  TA buffer + 0.1% CTAB, respectively. An important corollary consideration was the surface charge dependence of CTAB–protein complexes on buffer ionic strength,<sup>41,42</sup> as this dependence should also affect protein capture. Therefore, the relative magnitudes of surface charges for PG and BSA in the three buffer conditions were obtained for comparison using Menon's approach<sup>43</sup> (see Supporting Information). For PG, the surface charge ratios were 2.30, 1.0, and 0.65, and for BSA, they were 2.38, 1.0, and 0.65 for 7.57 $\times$ , 1.0 $\times$ , and 0.13 $\times$  buffer concentrations, respectively (Table S-2, Supporting Information); the surface charge increased as ionic strength increased. As shown in Figure 1c, even with increasing surface charge, protein capture decreased with increasing buffer ionic strength (enhanced charge shielding). The trend observed here supports the hypothesis that electrostatic interaction is the dominant mechanism of protein capture on the EIG.<sup>38,39</sup> Through the charge interaction studies, we noted that the capture efficiency can be adjusted by charge density and/or buffer ionic strength. For development of the WB assay with an integrated EIG region for pan-analyte capture, we selected EIG copolymerized with 1.6  $\mu$ M  $\beta$ -gal, owing to the high protein capture efficiency (Figure 1b).

**Demonstration and Characterization of Microfluidic WB Assay Integrated with EIG.** After establishing the protein immobilization performance, we integrated the EIG with CTAB-PAGE to yield an integrated microfluidic WB (Figure 2b). As detailed in Figure 2c, the microfluidic device seamlessly integrates five WB assay steps: (1) electrophoretic injection of a narrow protein sample zone, (2) CTAB-PAGE, (3) electrotransfer and electrostatic protein blotting, (4) blocking of nonspecific antibody binding sites on EIG, and (5) antibody-based probing of all immobilized protein bands. Step 1 initiated with "priming" of the separation axis (Figure 2b) with run buffer 1 $\times$  TA + 0.1% CTAB. After priming, protein ladder was electrophoretically loaded to a double-T injection junction (Figure 2a) to create and inject a narrowly defined

protein zone (plug). The protein ladder consisted of 200 nM each of PG, OVA, BSA, and  $\alpha A$ . The protein plug was injected along the separation axis. In contrast to an SDS-PAGE system,<sup>2</sup> positively charged CTAB–protein complexes migrated from the anode to cathode. A discontinuous 3-to-6%T gel created a sample stacking interface at the head of the separation axis (Figure 2b) to minimize injection dispersion as CTAB-PAGE commenced; the injected analyte zone width, defined as  $\pm 2\sigma$  of a Gaussian fit, was reduced by 57% (493 to 213  $\mu\text{m}$ ) upon electromigration through the stacking interface.

Step 2 commenced when the sample plug entered the separation gel (6%T). CTAB-PAGE separated proteins and yielded protein size information. Upon application of an electric field ( $E = 47 \text{ V}\cdot\text{cm}^{-1}$ ), the protein ladder was fully resolved (i.e., separation resolution or  $SR \geq 1.5$  for the least resolved BSA-OVA peaks) in an elapsed time of 36 s (Figure 3a). The separation length needed for completion of the sizing assay was 1496  $\mu\text{m}$ , defined by the fastest peak position (PG) when the least resolved peak pair was at  $SR = 1.5$ . Both the fast sizing and short separation distances needed were attributed to the low injection dispersion by stacking and reasonably high electric field. Separation of the protein ladder yielded a log–linear  $M_r$  vs mobility relation ( $y = -1.96 \times 10^3 x + 5.33$ ,  $R^2 = 0.997$ ,  $n = 5$ , Figure 3b).  $M_r$  of unknown species was also accurately predicted using a log–linear  $M_r$  vs mobility curve. In a separate PAGE experiment, five ladder proteins, S100B, OVA, BSA, phosphorylase b, and  $\beta\text{-gal}^*$ , were used to yield a log–linear  $M_r$  vs mobility relation. LF protein (78 kDa) comigrated with the ladder, and  $M_r$  of the LF was predicted using mobility data ( $M_r = 78.8 \text{ kDa}$ , 1.0% error).

Step 3 consists of transfer and blotting, which is composed of both electrophoretic transfer of sized species and pan-analyte protein capture on the EIG. For characterization of Step 3 and later steps, new ladder composition of PG (260 or 600 nM), OVA (220 nM), BSA (80 nM), and  $\beta\text{-gal}^*$  (100 nM) was used. Application of a transverse electric field across the micro-chamber (lateral dimension) allowed all sized proteins to be electrotransferred from the separation gel to the EIG in 31 s (Figure 3c). Electrostatic interaction with the EIG resulted in compression (i.e., enrichment, 25%, 56%, and 65% peak-width reduction for PG, OVA, and BSA, respectively) and subsequent immobilization of the sized analyte zones. The material retention on the EIG was 92%, 100%, 66%, and 21% for PG, OVA, BSA, and  $\beta\text{-gal}^*$ , respectively, at the immobilization (31 s time point). The capture efficiency in standard SDS slab gel and nitrocellulose membrane is observed to be comparable: ranging from 89 to 29% for 30 to 98 kDa proteins.<sup>44</sup> In contrast to previous work<sup>13,14</sup> where only one or two targeted analyte(s) was captured in each blotting region, all CTAB–protein complexes were immobilized. Consequently, probing is analogous to conventional WB in that detection antibodies in free solution (i.e., not copolymerized matched pair antibody) are introduced to the blotting membrane (EIG) after electrotransfer. During electrotransfer, a portion of select high surface charge proteins (e.g.,  $\beta\text{-gal}^*$ , BSA) was retained in the CTAB-PAGE separation gel. We speculate that the retention arises from protein interaction with hydrolyzed PA gel.<sup>28–30</sup>

Immobilization of analytes with minimal loss of sizing information is crucial for WB. SR losses from CTAB-PAGE to immobilization on the EIG were 1.5% to 10%; see variation SR values in fluorescence intensity graphs of Figure 3c and in Table S-3, Supporting Information. Both the capture efficiency and the penetration distance into the EIG can be optimized for

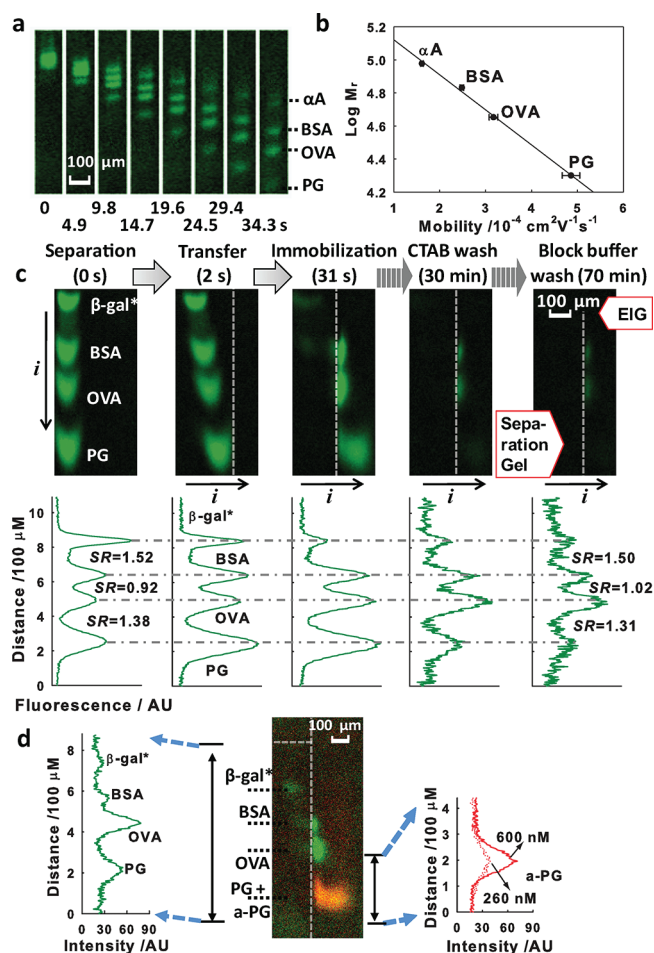


**Figure 3.** Microfluidic WB using EIG for protein capture allows fully integrated WB for probing of all sized proteins. (a) Time evolution of CTAB-PAGE sizing for four  $M_r$  standard proteins. (b) Corresponding log–linear  $M_r$  vs mobility plot. (c) After separation, electrotransfer of sized species to the EIG results in protein band capture for subsequent electrophoretically driven blocking, washing, and antibody probing. The elapsed time from the beginning of the assay (PAGE initiation) is indicated. Appended fluorescence intensity graphs (scaled for the maximum peak at each step) and SR values show conservation of sizing information throughout the assay. (d) Multispectral image (center) shows that PG (green fluor) is specifically detected among other immobilized proteins (left) using antibody probe a-PG (red fluor). Signal from probing antibody (right) decreases for samples with lower starting target concentration.

each analyte. PG, the smallest  $M_r$  species (lowest surface charge), was retained well (200  $\mu\text{m}$  penetration distance) within the width of the EIG (550  $\mu\text{m}$ ). An increased charge density on the EIG would likely result in higher capture efficiency and shorter penetration depths for smaller  $M_r$  species (e.g., <20 kDa). Alternatively, wider EIG regions can be fabricated.

In Step 4, a lateral electric field ( $E = 45 \text{ V}\cdot\text{cm}^{-1}$ ) was applied to drive free CTAB out of the EIG and introduce blocking reagent. Prior to commencing this step, fresh buffer solution was added to access holes #6 and #7 (Figure 2a). Step 4 prepared the EIG for subsequent introduction of probing (detection) antibodies. The electrophoretic “wash” to remove free CTAB minimized association of CTAB with antibody probes, introduced in Step 5. CTAB complexing with antibody probes contributed to significant background signal.<sup>24</sup> During

the extended application of the electric field for the wash step (30 min), material capture was reduced to 11%, 29%, 13%, and 5% for PG, OVA, BSA, and  $\beta$ -gal\*, respectively, because of competition between off rate of the protein binding to the EIG and electromigration out of the microchamber. Similar material reduction has been observed during electrotransfer to nitrocellulose membranes in conventional slab-gel WB.<sup>45</sup> To block nonspecific antibody binding EIG sites, unlabeled 1% w/v BSA was electrophoretically injected to the EIG for 15 min ( $E = 45 \text{ V}\cdot\text{cm}^{-1}$ ) using reverse polarity (i.e., BSA is negatively charged in nondetergent condition). After the 10 min blocking incubation, a reverse field was applied for 15 min to remove unbound blocking BSA. Material retention was reduced (6%, 19%, 8%, and 5% for PG, OVA, BSA, and  $\beta$ -gal\*, respectively). After the final blocking-BSA wash, however, no further appreciable material reduction was observed (Figure S-5, Supporting Information). Optimization of the CTAB wash and blocking step durations is underway and is anticipated to improve material retention and assay sensitivity.

In Step 5, proteins immobilized on the EIG were probed with fluorescently labeled detection antibodies. Antibodies conjugated with red fluorophores (Alexa Fluor 568) were electrophoretically introduced to the EIG for 15 min, incubated for 10 min, and unbound antibody was washed for  $\sim 15$  min. Figure 3d reports probing results for 200 nM antibody bound to immobilized 600 nM PG. Red signal from the antibody was specific for the PG peak with an acceptable background (SNR = 34), 11 min after commencing the antibody wash. The SNR for the immobilized proteins conjugated with green fluorophore (Alexa Fluor 488) is acceptable even after almost 2 h of electric field application: 6, 16, 8, and 5 for PG, OVA, BSA, and  $\beta$ -gal\*, respectively. Antibody probing of PG at two concentrations (600 vs 260 nM) reveals a concomitant response of probing antibody signal (1278 vs 637), suggesting that protein quantitation may be possible.

Antibody probing did not include a separate protein renaturation step required for conventional SDS slab-gel WB. Elimination of a specific renaturation step was anticipated, owing to the reports that CTAB-treated proteins retain native functions,<sup>22–24</sup> as is advantageous for assay design. Conventional renaturation strategies, including filtration, dilution, and dialysis are not suitable for low-dispersion, multistage microfluidic assays, as integration is difficult and losses are not well controlled. Compared with conventional slab-gel WB, performance of the microfluidic WB format was notably advanced in all assay steps, as tabulated in the performance characterization summary (Table 1).

**Lactoferrin Detection in Human Tear Fluids Using EIG-Based Microfluidic WB.** Immunoblotting assays are useful for the study of protein biomarkers of disease and dysfunction. Consequently, the microfluidic WB was implemented for the analysis of lactoferrin (LF), a putative biomarker for Sjögren's syndrome (SS), an autoimmune disease where immune cells attack exocrine glands.<sup>49</sup> PAGE analysis of LF in nondetergent conditions has been challenging due to the high pI (8.7) and a tendency for LF to nonspecifically associate with other proteins and substrates.<sup>25,50,51</sup> While ELISA is often used to assess LF in human tears, nonspecific interactions with ELISA microplates may yield high backgrounds.<sup>52</sup> Also, sizing information from CTAB-PAGE would improve assay specificity over ELISA. Bjerrum employed SDS-PAGE to assess the ratio of separated albumin and LF proteins in tears of SS patients and other

**Table 1. Performance Comparison of Slab-Gel and Microfluidic Western Blotting (WB)**

step	metric	slab-gel WB	microfluidic WB
loading	sample consumption	1–40 $\mu\text{g}$	0.01–0.5 $\mu\text{g}$ (loaded mass) <sup>a</sup>
	duration	2 h	3 min
separation	plate number (N)	$\sim 1000$ <sup>46</sup>	2690 (PG), 486 (OVA)
	mobility variation	10% <sup>47</sup>	2.2–4.3%
	capture efficiency	29–89% <sup>44,b</sup>	21–100% <sup>c</sup>
transfer and immobilization	duration	2 h	1 min
	SR variation	15% <sup>13</sup>	1.5–10%
immunodetection	duration	6–8 h	$\sim 2 \text{ h}$ <sup>d</sup>
	LOD	1 ng <sup>48,e</sup>	$\sim 1 \text{ ng}$ <sup>f</sup>

<sup>a</sup>Mass of material actually injected to the microchamber is 0.5–25 pg. <sup>b</sup>30 to 98 kDa proteins. <sup>c</sup>Initial capture efficiency. <sup>d</sup>Duration not optimized. <sup>e</sup>Detected using fluorescently labeled primary antibody, scanned on a fluorescence scanner. <sup>f</sup>Based on the loaded mass.

connective tissue diseases, and used the ratio as a diagnostic test of SS.<sup>53</sup>

The CTAB microfluidic WB assay was optimized to assess LF. For assaying LF in  $1\times$  TA buffer, an increased CTAB concentration (0.5%) was used to prime the separation axis. Higher CTAB concentrations afforded separations with minimal dispersion, as the interaction of LF with the PA separation gel was reduced. Without a proper priming, LF was observed to nonspecifically associate with the PA gel, agreeing with previous findings.<sup>51</sup> After an antibody screening, carrier-free goat polyclonal antihuman LF antibody was determined to provide a reliable blotting signal. Optimization of the blocking buffer yielded selection of diluted BSA (0.2%). Figure 4a shows

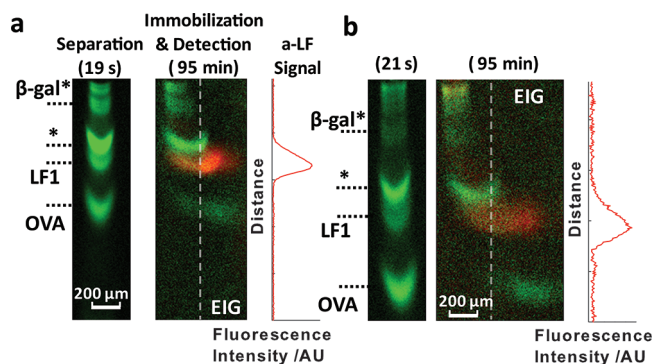


**Figure 4.** Microfluidic WB with EIG for pan-analyte capture allows assessment of LF. CTAB-PAGE separation and immunoblot readout of  $M_r$  standards and human LF in (a)  $1\times$  TA buffer and (b) diluted human tear fluid.

the results for an ideal system of LF purified from human breast milk (400 nM) spiked into  $1\times$  TA buffer + 0.2% CTAB along with a protein ladder consisting of OVA (150 nM) and  $\beta$ -gal\* (600 nM). At 16 s elapsed separation time ( $E = 84 \text{ V}\cdot\text{cm}^{-1}$ ), CTAB-PAGE resolved LF from the OVA and  $\beta$ -gal\* (SR  $\geq 1.5$ ). We noted that an unresolved peak (\*) about 85 kDa migrated closely with the LF peak. The source of the unidentified peak (\*) was the  $\beta$ -gal\* sample. After blotting, the antibody (red fluor) bound to LF (SNR = 275, 5 min after commencing antibody wash step).

After establishing baseline conditions for successful detection of LF in a TA buffer, LF in a complex biological matrix was assayed. For assay of LF in human tear fluid, 0.5% CTAB was also used to prime the separation axis. LF (400 nM) was spiked in LF-depleted human tear fluid (48× diluted with 1× TA buffer). Owing to the high background of proteins in tears (~500 species, total 8 mg/mL),<sup>27</sup> CTAB in the sample buffer was increased to 0.7% to improve detergent association. At 14 s of elapsed separation time and 992 μm of separation length ( $E = 60 \text{ V}\cdot\text{cm}^{-1}$ ), LF was fully resolved from the comigrating protein ladder OVA and β-gal\* (Figure 4b) with the exception of the peak (\*). The LF band was selectively immunoblotted by the antibody probe yielding an SNR of 43 (5 min after commencing antibody wash step). Study of endogenous LF expression in healthy and SS patient cohorts are underway.

## CONCLUSIONS

We introduced and characterized a PA gel immobilization matrix (EIG) for electrostatic capture of proteins and employed the novel material to yield an integrated microfluidic WB capable of pan-analyte protein immobilization for antibody probing after detergent-based sizing. Detailed binding-mechanism studies suggested an electrostatic interaction between CTAB-laden proteins and the charge-patterned EIG. Although demonstrated for proteins, the EIG could be readily extended to immobilize and assay other important charged biomolecules such as DNA and RNA. A cationic detergent buffer system (CTAB-Tricine-arginine) yielded accurate  $M_r$  information and was compatible with subsequent antibody probing without a time-consuming and dispersive protein renaturation process. The EIG-integrated microfluidic WB afforded a key advantage over previous approaches;<sup>13–15</sup> the EIG enabled immobilization of all sized proteins, making the present approach directly analogous to slab-gel WB as copolymerization of capture antibody was not needed. Detection using a secondary antibody and signal amplification through enzymatic reactions is feasible, and development is underway.

The integrated WB assay was demonstrated for assessment of LF in human tear fluid and yielded significant improvements in assay speed, sample/reagent consumption, reproducibility, and assay automation compared to conventional slab-gel WB. The small microchamber of our WB device allowed consumption of ~10<sup>5</sup>-fold less material to fabricate gels and blotting membranes than traditional WB. Biological (e.g., heparin) and synthetic macropolymers (e.g., polyacrylate sodium salt<sup>54</sup>) are under investigation as inexpensive alternative capture moieties. Taken together, we anticipate broad applicability of the microfluidic WB in general biology or clinical laboratory settings. The automated, multistage microfluidic CTAB Western blotting forms a versatile platform technology for advancing to an era of “high throughput” proteomics.

## ASSOCIATED CONTENT

### Supporting Information

Epi-fluorescence microscopy movie of a protein separation, transfer, and electrostatic blotting sequence. Additional information on microfluidic WB chip fabrication and the EIG characterization study. Additional detail on voltage and current sequence for the automated WB assay. Additional information on characterization of protein transfer and immobilization. This material is available free of charge via the Internet at <http://pubs.acs.org/>

## AUTHOR INFORMATION

### Corresponding Author

\*E-mail: [aeh@berkeley.edu](mailto:aeh@berkeley.edu). Phone: (510) 666-3396. Fax: (510) 642-5835.

### Notes

The authors declare no competing financial interest.

## ACKNOWLEDGMENTS

The authors gratefully acknowledge Dr. Nancy McNamara (UCSF Proctor Eye Foundation) for providing patient tear samples. This work was supported by the University of California (UC) Discovery Grant and the Industry-University Cooperative Research Program (IUCRP). A.E.H. is an Alfred P. Sloan Foundation Research Fellow in chemistry.

## REFERENCES

- (1) Ursula, B. *Anal. Chim. Acta* **2006**, *568*, 232–247.
- (2) Laemmli, U. K. *Nature* **1970**, *227*, 680–685.
- (3) Towbin, H.; Staehelin, T.; Gordon, J. *Proc. Natl. Acad. Sci.* **1979**, *76*, 4350–4354.
- (4) Ciaccio, M. F.; Wagner, J. P.; Chuu, C.; Lauffenburger, D. A.; Jones, R. B. *Nat. Methods* **2010**, *7*, 148–155.
- (5) MacBeath, G.; Schreiber, S. L. *Science* **2000**, *289*, 1760–1763.
- (6) Hu, S.; Xie, Z.; Qian, J.; Blackshaw, S.; Zhu, H. *Wiley Interdiscip. Rev. Syst. Biol. Med.* **2011**, *3*, 255–268.
- (7) Pollard, H. B.; Srivastava, M.; Eidelman, O.; Jozwik, C.; Rothwell, S. W.; Mueller, G. P.; Jacobowitz, D. M.; Darling, T.; Guggino, W. B.; Wright, J.; Zeitlin, P. L.; Paweletz, C. P. *Proteomics Clin. Appl.* **2007**, *1*, 934–952.
- (8) Rubina, A. Y.; Kolchinsky, A.; Makarov, A. A.; Zasedatelev, A. S. *Proteomics* **2008**, *8*, 817–831.
- (9) Pruthi, R. K.; Daniels, T. M.; Heit, J. A.; Chen, D.; Owen, W. G.; Nichols, W. L. *Thromb. Res.* **2010**, *126*, 543–549.
- (10) Desai, S.; Dworecki, B.; Cichon, E. *Anal. Biochem.* **2001**, *297*, 94–98.
- (11) Yershov, G.; Barsky, V.; Belgovskiy, A.; Kirillov, E.; Kreindlin, E.; Ivanov, I.; Parinov, S.; Guschin, D.; Drobishev, A.; Dubiley, S.; Mirzabekov, A. *Proc. Natl. Acad. Sci.* **1996**, *93*, 4913–4918.
- (12) He, M.; Novak, J.; Julian, B. A.; Herr, A. E. *J. Am. Chem. Soc.* **2011**, *133*, 19610–19613.
- (13) He, M.; Herr, A. E. *J. Am. Chem. Soc.* **2010**, *132*, 2512–2513.
- (14) Tia, S. Q.; He, M.; Kim, D.; Herr, A. E. *Anal. Chem.* **2011**, *83*, 3581–3588.
- (15) He, M.; Herr, A. E. *Nat. Protoc.* **2010**, *5*, 1844–1856.
- (16) Arenkov, P.; Kukhtin, A.; Gemmell, A.; Voloshchuk, S.; Chupeeva, V.; Mirzabekov, A. *Anal. Biochem.* **2000**, *278*, 123–131.
- (17) Anderson, G. J.; Cipolla, C. M.; Kennedy, R. T. *Anal. Chem.* **2011**, *83*, 1350–1355.
- (18) Pan, W.; Chen, W.; Jiang, X. *Anal. Chem.* **2010**, *82*, 3974–3976.
- (19) Williams, J. G.; Gratzner, W. B. *J. Chromatogr., A* **1971**, *57*, 121–125.
- (20) Marjanen, L. A.; Ryrle, I. J. *Biochim. Biophys. Acta, Protein Struct.* **1974**, *371*, 442–450.
- (21) Eley, M. H.; Burns, P. C.; Kannapell, C. C.; Campbell, P. S. *Anal. Biochem.* **1979**, *92*, 411–419.
- (22) Akins, R. E.; Levin, P. M.; Tuan, R. S. *Anal. Biochem.* **1992**, *202*, 172–178.
- (23) Akin, D. T.; Shapira, R.; Kinkade, J. M. *Anal. Biochem.* **1985**, *145*, 170–176.
- (24) Buxbaum, E. *Anal. Biochem.* **2003**, *314*, 70–76.
- (25) Karns, K.; Herr, A. E. *Anal. Chem.* **2011**, *83*, 8115–8122.
- (26) Hou, C.; Herr, A. E. *Anal. Chem.* **2010**, *82*, 3343–3351.
- (27) de Souza, G. A.; de Godoy, L.; Mann, M. *Genome Biol.* **2006**, *7*, R72.1–R72.11.
- (28) Kurenkov, V. F.; Hartan, H.-G.; Lobanov, F. I. *Russ. J. Appl. Chem.* **2001**, *74*, 543–554.

- (29) Nagase, K.; Sakaguchi, K. *J. Polym. Sci., Part A* **1965**, *3*, 2475–2482.
- (30) St Kenyeres, J.; Ursu, V. *J. Polym. Sci., Part A* **1980**, *18*, 275–281.
- (31) Huang, L. R.; Tegenfeldt, J. O.; Kraeft, J. J.; Sturm, J. C.; Austin, R. H.; Cox, E. C. *Nat. Biotechnol.* **2002**, *20*, 1048–1051.
- (32) Luther, J. R.; Glatz, C. E. *Biotechnol. Bioeng.* **1994**, *44*, 147–153.
- (33) Roth, C. M.; Lenhoff, A. M. *Langmuir* **1993**, *9*, 962–972.
- (34) Zilberstein, G.; Korol, L.; Znaleziona, J.; Sebastiano, R.; Righetti, P. G.; Shlar, I.; Baskin, E.; Bukshpan, S. *Anal. Chem.* **2008**, *80*, 5031–5035.
- (35) Holmes, D. L.; Stellwagen, N. C. *Electrophoresis* **1991**, *12*, 612–619.
- (36) Hamilton, R. G.; Roebber, M.; Reimer, C. B.; Rodkey, L. S. *Electrophoresis* **1987**, *8*, 127–134.
- (37) Chen, W.; Huang, H.; Lin, C.; Lin, F.; Chan, Y. *Langmuir* **2003**, *19*, 9395–9403.
- (38) Schreiber, G.; Fersht, A. R. *Nat. Struct. Mol. Biol.* **1996**, *3*, 427–431.
- (39) Zhou, H. *Biopolymers* **2001**, *59*, 427–433.
- (40) Lan, Q.; Bassi, A. S.; Zhu, J.; Margaritis, A. *Chem. Eng. J.* **2001**, *81*, 179–186.
- (41) Maulik, S.; Dutta, P.; Chattoraj, D. K.; Moulik, S. P. *Colloids Surf., B* **1998**, *11*, 1–8.
- (42) Subramanian, M.; Sheshadri, B. S.; Venkatappa, M. P. *J. Biochem. (Tokyo)* **1984**, *95*, 413–421.
- (43) Menon, M. K.; Zydney, A. L. *Anal. Chem.* **1998**, *70*, 1581–1584.
- (44) Olsen, I.; Wiker, H. G. *J. Immunol. Methods* **1998**, *220*, 77–84.
- (45) Bolt, M. W.; Mahoney, P. A. *Anal. Biochem.* **1997**, *247*, 185–192.
- (46) Han, J.; Singh, A. K. *J. Chromatogr., A* **2004**, *1049*, 205–209.
- (47) Scherberich, J. E.; Fischer, P.; Bigalke, A.; Stangl, P.; Wolf, G. B.; Haimerl, M.; Schoeppe, W. *Electrophoresis* **1989**, *10*, 58–62.
- (48) Bergendahl, V.; Glaser, B. T.; Burgess, R. R. *J. Immunol. Methods* **2003**, *277*, 117–125.
- (49) Ohashi, Y.; Ishida, R.; Kojima, T.; Goto, E.; Matsumoto, Y.; Watanabe, K.; Ishida, N.; Nakata, K.; Takeuchi, T.; Tsubota, K. *Am. J. Ophthalmol.* **2003**, *136*, 291–299.
- (50) Hekman, A. *Biochim. Biophys. Acta, Protein Struct.* **1971**, *251*, 380–387.
- (51) Malmquist, J.; Johansson, B. G. *Biochim. Biophys. Acta, Protein Struct.* **1971**, *236*, 38–46.
- (52) Rebeski, D. E.; Winger, E. M.; Shin, Y.; Lelenta, M.; Robinson, M. M.; Varecka, R.; Crowther, J. R. *J. Immunol. Methods* **1999**, *226*, 85–92.
- (53) Bjerrum, K. B. *Acta Ophthalmol. Scand.* **1997**, *75*, 507–511.
- (54) Bordi, F.; Cametti, C.; Diociaiuti, M.; Gaudino, D.; Gili, T.; Sennato, S. *Langmuir* **2004**, *20*, 5214–5222.